HHS Public Access

Author manuscript

Mol Imaging Biol. Author manuscript; available in PMC 2021 February 01.

Published in final edited form as:

Mol Imaging Biol. 2020 February ; 22(1): 134–143. doi:10.1007/s11307-019-01356-z.

Radiofluorinated GPC3-Binding Peptides for PET Imaging of Hepatocellular Carcinoma

Youcai Li[#1,3], **Jun Zhang**[#2,4], **Jiamei Gu**[1], **Kongzhen Hu**[1], **Shun Huang**[1], **Peter S. Conti**[2], **Hubing Wu**[1,2], **Kai Chen**[2]

[1]Nanfang PET Center, Nanfang Hospital, Southern Medical University, 1838 Guangzhou Avenue North, Guangzhou, 510515, Guangdong Province, China

[2]Molecular Imaging Center, Department of Radiology, Keck School of Medicine, University of Southern California, 2250 Alcazar Street, CSC103, Los Angeles, CA, 90033, USA

[3]PET/CT Center, The First Affiliated Hospital of Guangzhou Medical University, Guangzhou, Guangdong Province, China

[4]Department of Nuclear Medicine, Taizhou People's Hospital, Taizhou, Jiangsu Province, China

[#] These authors contributed equally to this work.

Abstract

Purpose: Hepatocellular carcinoma (HCC) remains one of the most challenging diseases worldwide. Glypican-3 (GPC-3) is a cell surface proteoglycan that is overexpressed on the membrane of HCC cells. The purpose of this study was to develop a target-specific radiofluorinated peptide for positron emission tomography (PET) imaging of GPC3 expression in hepatocellular carcinoma.

Procedures: New GPC3-binding peptides (GP2076 and GP2633) were radiolabeled with F-18 using Al[^{18}F]F labeling approach, and the resulting PET probes were subsequently subject to biological evaluations. A highly hydrophilic linker was incorporated into GP2633 with an aim of reducing the probe uptake in liver and increasing tumor-to-liver (T/L) contrast. Both GP2076 and GP2633 were radiolabeled using Al[^{18}F]F chelation approach. The binding affinity, octanol/water partition coefficient, cellular uptake and efflux, and stability of both F-18 labeled peptides were tested. Tumor targeting efficacy and biodistribution of Al[^{18}F]F-GP2076 and Al[^{18}F]F-GP2633 were determined by PET imaging in HCC-bearing mice. Immunohistochemistry analyses were performed to compare the findings from PET scans.

Correspondence to: Hubing Wu; wuhbym@163.com, Kai Chen; chenkai@med.usc.edu.

Conflict of Interest

The authors declare that they have no conflict of interest.

Compliance with Ethical Standards.

All animal studies were approved by the Nanfang Hospital Animal Ethics Committee at the Southern Medical University, and in accordance with its guidelines.

Electronic supplementary material The online version of this article (https://doi.org/10.1007/s11307-019-01356-z) contains supplementary material, which is available to authorized users.

Publisher's Note. Springer Nature remains neutral with regard to jurisdictional claims in published maps and institutional affiliations.

Results: Al[^{18}F]F-GP2076 and Al[^{18}F]F-GP2633 were rapidly radiosynthesized within 20 min in excellent radiochemical purity (> 97 %). Al[^{18}F]F-GP2633 was determined to be more hydrophilic than Al[^{18}F]F-GP2076 in terms of octanol/water partition coefficient. Both Al[^{18}F]F-GP2076 and Al[^{18}F]F-GP2633 demonstrated good *in vitro* and *in vivo* stability and binding specificity to GPC3-positive HepG2 cells. For PET imaging, Al[^{18}F]F-GP2633 exhibited enhanced uptake in HepG2 tumor (%ID/g 3.37 ± 0.35 *vs.* 2.13 ± 0.55, $P = 0.031$) and reduced accumulation in liver (%ID/g 1.70 ± 0.26 *vs.* 3.70 ± 0.98, $P = 0.027$) at 60 min post-injection (pi) as compared to Al[^{18}F]F-GP2076, resulting in significantly improved tumor-to-liver (T/L) contrast (ratio 2.00 ± 0.18 *vs.* 0.59 ± 0.14, $P = 0.0004$). Higher uptake of Al[^{18}F]F-GP2633 in GPC3-positive HepG2 tumor was observed as compared to GPC3-negative McA-RH7777 tumor (%ID/g 3.37 ± 0.35 *vs.* 1.64 ± 0.03, $P = 0.001$) at 60 min pi, confirming GPC3-specific accumulation of Al[^{18}F]F-GP2633 in HepG2 tumor.

Conclusion: The results demonstrated that Al[^{18}F]F-GP2633 is a promising probe for PET imaging of GPC3 expression in HCC. Convenient preparation, excellent GPC3 specificity in HCC, and favorable excretion profile of Al[^{18}F]F-GP2633 warrant further investigation for clinical translation. PET imaging with a GPC3-specific probe would provide clinicians with vital diagnostic information that could have a significant impact on the management of HCC patients.

Keywords

GPC3; Hepatocellular carcinoma; PET imaging; F-18 labeled peptides; Hydrophilic linker

Introduction

Liver cancer is a major health problem, which currently ranks the fourth leading cause of cancer death worldwide [1]. Among all primary liver cancers, hepatocellular carcinoma (HCC) is the most common type, representing 75 %–85 % of all primary liver cancer cases [1, 2]. In the USA, HCC incidence and mortality rates have been increasing for decades [3]. A median survival following diagnosis of HCC is approximately 6 to 20 months due to late diagnosis in its course and few effective treatment options [4, 5]. Although surgical resection or liver transplantation may sometimes be successful for the treatment of early-stage HCC, very limited treatment options are available for patients diagnosed at an advanced stage [5]. Definitive diagnosis *via* non-invasive testing of HCC in clinic includes four-phase multi-detector computed tomography (CT) or dynamic contrast-enhanced magnetic resonance imaging (MRI) [6]. Further improvement in HCC patient management through imaging will be limited unless anatomical studies are augmented with an assessment of tumor biology and metabolism *in vivo* [7]. A major factor contributed to this limitation is inability to characterize tumor growth and metabolism, a matter of pathophysiology which cannot be evaluated by anatomic imaging techniques. Targeted therapies for the management of patients with HCC continue to be researched [6]. However, the treatment responses are still being assessed on the basis of tumor size measurement before and after therapy. As targeted therapies may not cause significant changes in the size of lesions at an early stage, assessment of response to such treatments may not be accurate using conventional size measurement. The development of positron emission tomography (PET)/x-ray computed tomography (CT) technology creates the opportunity to combine metabolic and anatomic

imaging capabilities, capitalizing on the advantages each modality affords. A sizable body of evidence suggests that the basic pathophysiological processes of HCC may be evaluable *in vivo* using the physiologic imaging capabilities of PET [8-10]. Therefore, a target-specific PET probe may provide the early detection of HCC and/or be used as a companion diagnostic for HCC therapy.

Glypicans (GPCs) are a family of heparan sulfate proteoglycans anchored to cell membrane [11]. Among six identified GPCs in mammals [12], glypican-3 (GPC3) is an oncofetal proteoglycan containing a 70 kDa core protein [11]. There is no GPC3 expression in healthy liver, but GPC3 expression remains at high levels in HCCs [13]. In addition, the research results showed that, during the invasive growth of liver cancer, GPC3 expresses at different levels, suggesting that GPC3 plays an important role on HCC development [14]. Furthermore, HCC cell migration and invasion can be inhibited by GPC3 knockdown, indicating GPC3 may also critically involve in HCC metastasis and invasion [15].

Due to the important role of GPC3 in the HCC progression, various GPC3-targeted therapies have been developed, including antibodies, vaccines, immunotoxins, and genetic therapies [16, 17]. Companion diagnostics for antibody-based HCC therapies have been recently reported [18-20], where an anti-human GPC3 mAb (DFO-1G12) or αGPC3 IgG1 and the fragments were radiolabeled with ^{89}Zr for PET imaging of HepG2 tumors. Although ^{89}Zr-labeled GPC3 mAbs showed very good HCC targeting efficacy and specificity, the relatively large size of mAbs led to unfavorable *in vivo* pharmacokinetics (PK) and immunogenicity [20], which might limit their clinical applications.

Through screening of a peptide library using immuno-precipitation method, a tetrakaideca peptide (TP) carrying sequence RLNVGGTYGLTTRQ was identified as a specific ligand binding to GPC3 [21]. This ligand can block the binding of the FITC-labeled TP to GPC3-expressing cells, further indicating the specific binding of TP for GPC3. As compared to antibodies, peptides usually show less immunogenicity and toxicity, and the production cost of peptides is relatively lower [22-25]. Thus, it has become our great interest of utilizing the TP as a platform to build up GPC3-targeted PET probes. In our recent proof-of-concept work, we radiolabeled the TP with F-18 to form a PET probe for imaging GPC3-positive HCC tumors [26]. However, a low tumor-to-liver (T/L) ratio was observed due to high hepatobiliary excretion. In this study, we designed a new F-18-labeled PET probe by incorporating a hydrophilic peptide linker (GGGRDN) to the TP. The new PET probe could reduce the background radioactivity in liver and thus increase the T/L ratio. An F-18-labeled PET probe without the hydrophilic linker was also prepared for comparison.

Materials and Methods

Materials

All chemicals were purchased from commercial suppliers and used without further purification. The peptides (sequence: RLNVGGTYFLTTRQ) [21, 26] and GGGRDNRLNVGGTYFLTTRQ) were synthesized by the ChinaPeptides Company (Shanghai, China). Details of other materials and the HPLC methods are provided in electronic supplementary material (ESM).

Radiosynthesis and In Vitro Studies

The radiolabeling of the GP2076 or GP2633 peptide was carried out using Al[^{18}F]F chelation approach (Fig. 1) [26-29]. In brief, to a 5-ml vial containing 2 mM aluminum chloride (6 μl), glacial acetic acid (5 μl), and acetonitrile (334 μl) was added 250 μg of peptide (0.12 μmol of GP2076 or 0.09 μmol of GP2633) in 100 μl deionized (DI) water. After a rapid vibration, 40–50 μl of [^{18}F]fluoride (555–740 MBq) was added into the mixture. The vial was heated at 100 °C for 10 min. After cooling to room temperature, the mixture was diluted with 15 ml of DI water. The mixture was then passed through a Varian Bond Elut C_{18} column, and the column was followed by washing with 10 ml of PBS and 20 ml of water. Then, 0.4 ml of ethanol containing 10 mM of HCl was used to elute the product. After dilution with saline, the solution passed through a sterile filter and collected directly into a sterile product vial. The radiochemical purify of Al[^{18}F]F-GP2076 or Al[^{18}F]F-GP2633 was determined based on reverse-phase analytical HPLC. Detailed procedures for the measurement of lipophilicity (Log P), cell culture and animal models, binding assay, *in vitro* biocompatibility, cellular uptake studies, and *in vitro* stability are provided in ESM.

In Vivo Metabolic Stability

HepG2 tumor-bearing mice (n = 3/group) were intravenously injected with 5.55 MBq of Al[^{18}F]F-GP2076 or Al[^{18}F]F-GP2633. At 1 h after the injection, the mice were euthanized, and the HepG2 tumor, blood, liver, kidneys, and urine samples were collected. The study was performed according to the procedures reported previously [30, 31]. Briefly, the blood sample was immediately centrifuged for 5 min at 12,000 rpm. The HepG2 tumor, liver, and kidneys were homogenized and then centrifuged for 5 min at 12,000 rpm. The supernatant from each sample was passed through an ultrafiltration tube (Millipore, USA) and then centrifuged for 10 min at 12,000 rpm. The urine sample was diluted with 100 μl of PBS. The filtrate from each sample was injected into analytic HPLC. The HPLC eluents were collected with a fraction collector (one fraction/30 s), and the radioactivity of each fraction was measured by gamma counting.

MicroPET/CT Imaging and Biodistribution

MicroPET/CT scans were carried out using a Siemens Inveon PET/CT scanner (Siemens, Germany). Tumor-bearing mice (n = 3/group) were intravenously injected with 5.55 MBq of Al[^{18}F]F-GP2076 or Al[^{18}F]F-GP2633 under isoflurane anesthesia. A 10-min static PET scan for each animal was acquired at 30, 60, and 120 min after the injection. Three-dimensional-ordered subset expectation maximization (3D-OSEM) algorithm was used for the PET reconstruction, and CT was applied for attenuation correction. Detailed procedures for the microPET/CT imaging and biodistribution are provided in ESM.

Tumor Histopathology

The tumor (HepG2 or McA-RH7777) tissues were fixed in paraformaldehyde (4 %) for 24 h. The specimens were then dehydrated in ethanol, embedded in paraffin, and cut into thick sections (5 μm). The fixed sections were deparaffinized and hydrated according to a standard protocol and stained with hematoxylin and eosin (H&E) for observation. For analysis of GPC3 expression, sections were incubated with an anti-GPC3 antibody at a dilution of 1:150

at 4 °C overnight, and then incubated with a secondary antibody (K5007, polymer-HRP, DAKO, Denmark) at room temperature for 50 min.

Statistical Analysis

Quantitative data are reported as mean ± standard deviation (SD). Means were compared using one-way ANOVA and student's *t* test. All tests were performed using SPSS version 20.0 (IBM Corporation, Armonk, NY, USA). A *P* value of less than 0.05 was considered statistically significant, and the data were marked with (*) for $P < 0.05$, (**) for $P < 0.01$, and (***) for $P < 0.001$, respectively.

Results

Chemistry and Radiochemistry

Synthetic methods for GP2076, GP2633, and their corresponding Al^{19}F-labeled peptides are detailed in ESM. All peptides were obtained in good yield and characterized by mass spectrometry (Suppl. Fig. 1, see ESM). Under the identical analytical HPLC condition, the retention time of GP2076 was 14.5 min, while the retention time of GP2633 was 13.5 min (Suppl. Fig. 2 a1 and a2, see ESM).

Al[^{18}F]F-GP2076 and Al[^{18}F]F-GP2633 were rapidly radiosynthesized using the Al^{18}F chelation strategy and the solid-phase extraction (SPE) purification approach. The total synthesis time for Al[^{18}F]F-GP2633 and [^{18}F]Al[^{18}F]F-GP2076 was approximately 20 min. The radiochemical yields (decay-uncorrected) of Al[^{18}F]F-GP2076 and Al[^{18}F]F-GP2633 were 29.25 ± 1.81 % ($n = 3$) and 24.86 ± 7.99 % ($n = 3$), respectively. After the SPE purification, the radiochemical purities of Al[^{18}F]F-GP2076 and Al[^{18}F]F-GP2633 were larger than 97 % as determined by analytical HPLC. The retention times of Al[^{18}F]F-GP2076 and Al[^{18}F]F-GP2633 were 14.0 min and 13.2 min, respectively (Suppl. Fig. 2, see ESM). The specific activities of Al[^{18}F]F-GP2076 and Al[^{18}F]F-GP2633 were estimated to be 780.5–1536.5 MBq/μmol and 939.1–1363.8 MBq/μmol, respectively.

The log *P* values of Al[^{18}F]F-GP2076 and Al[^{18}F]F-GP2633 were – 2.10 ± 0.07 ($n = 4$) and – 2.42 ± 0.09 ($n = 4$), respectively (Suppl. Table 1, see ESM), indicating that Al[^{18}F]F-GP2633 is more hydrophilic than Al[^{18}F]F-GP2076.

Binding Assay

The binding affinity of GP2076 and GP2633 for GPC3 was determined by SPR method. The K_D values of GP2076 and GP2633 were calculated to be 101 nM and 63.3 nM, respectively, suggesting that the incorporation of a hydrophilic linker (GGGRDN) slightly enhances the peptide binding affinity to GPC3.

In Vitro Biocompatibility

The cytobiocompatibility of GP2076 and GP2633 was examined prior to *in vivo* evaluations. As shown in Suppl. Fig. 3(see ESM), the cell viabilities of HepG2 cells were larger than 90 % at all examined concentrations ranging from 120 to 840 μg/ml, demonstrating the excellent cytocompatibility of GP2076 and GP2633.

Cellular Uptake, Internalization, and Efflux

The cellular uptake, internalization, and retention of Al[^{18}F]F-GP2076 and Al[^{18}F]F-GP2633 were determined in GPC3-positive HepG2 and GPC3-negative McA-RH7777 HCC cells. The cellular uptake results showed that both Al[^{18}F]F-GP2076 and Al[^{18}F]F-GP2633 bind to GPC3-positive HepG2 cells very rapidly, and the binding reaches a plateau after 30-min incubation (Fig. 2a). At 60 min, the peak values of cell uptake were 1.08 ± 0.04 % for Al[^{18}F]F-GP2076 and 1.15 ± 0.05 % for Al[^{18}F]F-GP2633, respectively. No significant uptake difference ($P = 0.721$) was observed between Al[^{18}F]F-GP2076 and Al[^{18}F]F-GP2633 after 1 h incubation, suggesting that both Al[^{18}F]F-GP2076 and Al[^{18}F]F-GP2633 can bind to GPC3-positive HepG2 cells very well. On the other hand, in GPC3-negative McA-RH7777 cells, the cellular uptake values of Al[^{18}F]F-GP2633 were significantly lower than those in GPC3-positive HepG2 cells after 15 min incubation (Fig. 2a). For instance, at 60 min, the cellular uptake of Al[^{18}F]F-GP2633 in McA-RH7777 cells was 0.30 ± 0.03 %, which is significantly lower than the value (1.15 ± 0.05 %, $P = 0.002$) in HepG2 cells. For the cell efflux study, both Al[^{18}F]F-GP2076 and Al[^{18}F]F-GP2633 exhibits reasonable cell retention than Al[^{18}F]F-GP2076 in HepG2 cells (Fig. 2b). During the first 30 min, the efflux (off-target) rate of Al[^{18}F]F-GP2633 was relatively slower than that of Al[^{18}F]F-GP2076, suggesting that the binding of Al[^{18}F]F-GP2633 to GPC3 is slightly stronger than that of Al[^{18}F]F-GP2076. This result is consistent with the data from the GPC3 binding affinity determination. During 1 h study time, about 0.83 % (from 1.04 % to 0.21 %) and 0.86 % (from 1.13 % to 0.27 %) of radioactivity efflux were observed for Al[^{18}F]F-GP2076 and Al[^{18}F]F-GP2633, respectively. In GPC3-negative McA-RH7777 cells, Al[^{18}F]F-GP2633 showed poor cell retention property, and the radioactivity was rapidly washed out to the baseline within 5 min. Taken together, the cell uptake and efflux data demonstrated that the binding of Al[^{18}F]F-GP2633 to HepG2 cells is target specific, which is indeed mediated by GPC3. As shown in Suppl. Fig. 4 (see ESM), the internalization of both Al[^{18}F]F-GP2076 and Al[^{18}F]F-GP2633 in HepG2 cells at 2 h was very low (< 10 % of cell uptake).

In Vitro and In Vivo Stability

The *vitro* stability of [Al[^{18}F]F-GP2076 and Al[^{18}F]F-GP2633 was determined in PBS at room temperature and mouse serum at 37 °C after 2 h incubation. The stability was measured as percentage of intact radiotracer according to the HPLC analysis (Suppl. Fig. 5, see ESM). Overall, both Al[^{18}F]F-GP2076 and Al[^{18}F]F-GP2633 showed excellent stability in PBS and mouse serum. After 2 h incubation, > 95 % of Al[^{18}F]F-GP2076 and > 98 % of Al[^{18}F]F-GP2633 remained intact.

At 1 h after intravenous injection of Al[^{18}F]F-GP2076 or Al[^{18}F]F-GP2633 into tumor-bearing mice, the metabolic stability was examined in HepG2 tumor, blood, liver, kidneys, and urine. The samples were analyzed by HPLC, and the representative radioactivity eluent profiles are shown in Fig. 3. For Al[^{18}F]F-GP2076, the percentage of the parent F-18 labeled peptide was found to 97.69 ± 2.51 % in HepG2 tumor, 96.68 ± 1.55 % in blood, 96.06 ± 0.54 % in liver, 54.94 ± 2.12 % in kidneys, and 3.31 ± 0.20 % in urine, respectively (Fig. 3a). For Al[^{18}F]F-GP2633, the percentage of the intact radiotracer was determined to be 93.01 ± 2.98 % in HepG2 tumor, 93.57 ± 1.38 % in blood, 92.95 ± 2.77 % in liver, 7.70 ± 2.56 % in kidneys, respectively (Fig. 3b). No parent Al[^{18}F]F-GP2633 was identified in

urine at 1 h post-injection (pi). Overall, both Al[^{18}F]F-GP2076 and Al[^{18}F]F-GP2633 displayed similar metabolic stability in HepG2 tumor, blood, and liver. As compared to Al[^{18}F]F-GP2076, Al[^{18}F]F-GP2633 was readily catabolized in kidneys, leading to complete metabolite(s) in urine.

MicroPET/CT Imaging and Biodistribution

The tumor-targeting efficacy and biodistribution of Al[^{18}F]F-GP2076 and Al[^{18}F]F-GP2633 were examined in nude mice-bearing GPC3-positive HepG2- or GPC3-negatice McA-RH7777 tumor xenografts at multiple time points (30, 60, and 120 min) with static PET scans. All GPC3-positive HepG2 tumors were clearly visible at all time points measured after the injection of Al[^{18}F]F-GP2076 or Al[^{18}F]F-GP2633, whereas the GPC3-negative McA-RH7777 tumors showed minimal uptake of Al[^{18}F]F-GP2633. Representative whole-body coronal slices (CT, PET, and PET/CT fusion) containing tumors at 60 min pi are shown in Fig. 4. Representative whole-body coronal PET images of tumor-bearing mice at different time points are presented in Suppl. Fig. 6(see ESM). Although both Al[^{18}F]F-GP2076 and Al[^{18}F]F-GP2633 exhibited very good uptake in HepG2 tumors, it is worthy to note that the pharmacokinetic (PK) properties of Al[^{18}F]F-GP2076 and Al[^{18}F]F-GP2633 are significantly different as visualized by PET images. High liver uptake of Al[^{18}F]F-GP2076 was observed at all imaging time points, whereas the accumulated radioactivities in liver for Al[^{18}F]F-GP2633 remained at minimal levels (Fig. 4 and Suppl. Figs. 6and7, see ESM). Apparently, the clearance of Al[^{18}F]F-GP2633 from the mouse body is predominantly through the renal system, while the excretion of Al[^{18}F]F-GP2076 is primarily through the hepatic pathway.

The radioactivity accumulated in tumor and major organs was evaluated by measuring the ROIs of the entire organ for each PET scan. The quantitative data of Al[^{18}F]F-GP2076 and Al[^{18}F]F-GP2633 at 30, 60, 120 min pi are presented in Fig. 5 and Suppl. Tables 2-14 (see ESM). For the HepG2 tumor uptake, at 30 and 60 min pi, the values of Al[^{18}F]F-GP2633 were higher than those of Al[^{18}F]F-GP2076 (%ID/g in HepG2 tumor at 30 min: 3.13 ± 0.31 *vs.* 2.20 ± 0.36, $P = 0.027$; %ID/g in HepG2 tumor at 60 min: 3.37 ± 0.35 *vs.* 2.13 ± 0.55, $P = 0.031$). At 120 min pi, the HepG2 tumor uptake values (%ID/g) between Al[^{18}F]F-GP2076 (0.73 ± 0.32) and Al[^{18}F]F-GP2633 (1.30 ± 0.17) were not considered statistically significant ($P = 0.054$) (Fig. 5 and Suppl. Tables 2-3, see ESM). For the GPC3-negative McA-RH7777 tumor model, the tumor uptake values of Al[^{18}F]F-GP2633 (%ID/g: 1.75 ± 0.05 at 30 min, 1.64 ± 0.03 at 60 min, and 0.66 ± 0.06 at 120 min, respectively) were significantly lower than those in the GPC3-positive HepG2 tumor model (%ID/g: 3.13 ± 0.31 at 30 min, 3.37 ± 0.35 at 60 min, and 1.30 ± 0.17 at 120 min, respectively) (Fig. 5 and Suppl. Tables 2 and 9, see ESM). For the liver uptake, at 30 and 60 min pi, the values of Al[^{18}F]F-GP2633 were significantly lower than those of Al[^{18}F]F-GP2076 (%ID/g in liver at 30 min: 1.80 ± 0.36 *vs.* 5.10 ± 0.53, $P = 0.001$; %ID/g in liver at 60 min: 1.70 ± 0.26 *vs.* 3.70 ± 0.98, $P = 0.027$) (Fig. 5 and Suppl. Tables 2 and 4, see ESM). For the uptake in kidneys, at 30 and 60 min pi, the values of Al[^{18}F]F-GP2633 were remarkably greater than those of Al[^{18}F]F-GP2076 (%ID/g in kidneys at 30 min: 39.40 ± 0.98 *vs.* 9.83 ±3.69, $P = 0.0002$; %ID/g in kidneys at 60 min: 36.86 ± 2.05 *vs.* 7.03 ± 2.32, $P = 0.0001$) (Fig. 5 and Suppl. Tables 2 and 5, see ESM). For the uptake of Al[^{18}F]F-GP2633 in liver and kidneys,

no statistical difference was found between the GPC3-positive HepG2 and GPC3-negative McA-RH7777 tumor model at 30, 60, and 120 min pi (Fig. 5 and Suppl. Tables 2, 10, and 11, see ESM). Minimal uptake of Al[^{18}F]F-GP2076 or Al[^{18}F]F-GP2633 was found in other major organs, such as brain, heart, and lung. Particularly, the low uptake of radioactivity in bone for both Al[^{18}F]F-GP2076 and Al[^{18}F]F-GP2633 proved that the Al[^{18}F]F-NOTA chelation is stable and defluorination from the radiotracers did not occur *in vivo.*

Based on the quantitative data from the PET scans, the tumor-to-non-target (T/M, T/L, and T/K) ratios were calculated (Fig. 5 and Suppl. Tables 6-8 and 12-14, see ESM). At all measured time points, the values of T/M for Al[^{18}F]F-GP2633 were significantly greater than those for Al[^{18}F]F-GP2076 (T/M: 9.11 ± 0.79 *vs.* 5.56 ± 1.36 (P = 0.017) at 30 min, 12.17 ± 0.62 *vs.* 5.13 ± 2.08 (P = 0.005) at 60 min, and 6.20 ± 1.80 *vs.* 2.68 ± 0.29 (P = 0.029) at 120 min, respectively). Significantly higher T/L values were also observed for Al[^{18}F]F-GP2633 as compared to Al[^{18}F]F-GP2076 at all measured time points (T/L: 1.77 ± 0.20 *vs.* 0.43 ± 0.06 (P = 0.0004) at 30 min, 2.00 ± 0.18 *vs.* 0.59 ± 0.14 (P = 0.0004) at 60 min, and 1.28 ± 0.25 *vs.* 0.46 ± 0.40 (P = 0.039) at 120 min, respectively). At 60 min pi, the T/K value of Al[^{18}F]F-GP2633 (0.09 ± 0.01) was found to be significantly lower than that of Al[^{18}F]F-GP2076 (0.31 ± 0.04, P = 0.001). For the GPC3-negative McA-RH7777 tumor model, at 30 and 60 min pi, the T/M ratios of Al[^{18}F]F-GP2633 (T/M: 3.87 ± 1.97 at 30 min, and 6.20 ± 2.67 at 60 min, respectively) were significantly lower than those in the GPC3-positive HepG2 tumor model (T/M: 9.11 ± 0.79 (P = 0.013) at 30 min, and 12.17 ± 0.62 (P = 0.019) at 60 min, respectively) (Fig. 5 and Suppl. Table 12, see ESM). At 30, 60, and 120 min pi, the T/L and T/K values of Al[^{18}F]F-GP2633 in the HepG2 tumor model were all significantly higher than those in the McA-RH7777 tumor model (Fig. 5 and Suppl. Tables 13-14, see ESM). Overall, at 60 min pi, the best tumor-to-non-target contrast can be achieved for Al[^{18}F]F-GP2633 in the GPC3-positive HepG2 tumor model, which can be very well distinguished from two comparing groups: Al[^{18}F]F-GP2076 in the HepG2 tumor model and Al[^{18}F]F-GP2633 in the McA-RH7777 tumor model.

The data from the *ex vivo* biodistribution at 60 min pi are shown in Suppl. Table 15 (see ESM). Overall, the results are consistent with the findings from the PET study. The HepG2 tumor uptake of Al[^{18}F]F-GP2633 was 1.96 ± 0.29 %ID/g which is significantly higher than that of Al[^{18}F]F-GP2076 (1.13 ± 0.02 %ID/g, P = 0.007). As compared to Al[^{18}F]F-GP2076, Al[^{18}F]F-GP2633 exhibited lower uptake in the liver (0.97 ± 0.07 %ID/g *vs.* 2.30 ± 0.56 %ID/g, P = 0.015). No statistical difference was observed for the tracer uptake in blood, heart, and bone between the Al[^{18}F]F-GP2076 and Al[^{18}F]F-GP2633 groups.

Tumor Histopathology

Qualitative visual assessment of the immunohistochemical assay showed high expression of GPC3 in the HepG2 xenograft (Fig. 6a) whereas the GPC3 expression in McA-RH7777 tumor was minimal (Fig. 6b). Hematoxylin and eosin (H&E) staining demonstrated that no tumor tissue damage was detected in both HepG2 and McA-RH7777 xenograft (Fig. 6c, d).

Discussion

Recent studies have shown that GPC3 plays a critical role on molecular mechanisms by which the proliferation and invasion of HCC are regulated and controlled [32]. The involvement of GPC3 in HCC progression was found through various pathways, including stimulation of Wnt signaling and macrophage recruitment, interaction with growth factors, and promotion of epithelial–mesenchymal transition [32, 33]. It is worthy to note that GPC3 expression levels are significantly different between the tumor tissue in HCCs and the tissue in healthy or nonmalignant livers. For example, in a clinic study [13], GPC3 expression was detected in 72 % of HCC patients, whereas no GPC3 expression was found in patients with a healthy or benign liver. In addition, GPC3 expression was identified in 63–91 % of HCC patients in approximate 20 clinical studies [16]. As a result, GPC3 has been considered as a valuable biomarker for the HCC diagnosis and therapy [16]. As the development of GPC3-targeted therapies continues to be a very active field of HCC treatment, studying GPC3-targeted PET imaging probes as companion diagnostics has become of great interest [18-20]. A GPC3-targeted PET probe can be used to noninvasively monitor the GPC3 expression during the tumorigenesis and HCC development and guide the GPC3-targeted treatment. In addition, due to overexpression of GPC3 in early-staged HCCs and minimal GPC3 expression in cirrhotic tissue, a GPC3-targeted PET probe could be useful in distinguishing the early-staged HCC from benign cirrhotic nodule, which remains a clinical challenge on the HCC diagnosis.

In our previous study, we prepared a peptide-based PET probe for imaging GPC3 expression in HepG2 tumors [26]. Although HepG2 tumors can be visualized by PET, the T/L ratio was low (0.93 ± 0.16) at 1 h pi. Predominant hepatobiliary excretion of the probe causes high radioactivity background in liver, which may hamper the detection of intrahepatic tumor as well as tumor in the abdomen. Low radioactivity background in liver is preferred for a PET probe to be sensitive enough to detect HCCs and/or hepatic metastases. Efforts have been made in the development of PET probes to reduce the hepatobiliary excretion and decrease the radioactivity level in liver [34-36]. One of effective approaches is to increase the hydrophilicity of PET probes by incorporating hydrophilic auxiliaries, such as a carbohydrate moiety, a polyethylene glycol (PEG) unit, and a peptide-based linker [34-36]. For instance, a linker with six hydrophilic amino acids (GGGRDN) containing no net charge was introduced to modify F-18-labeled GRPR agonists and antagonists [37]. Incorporating this linker into PET probes takes advantages of (1) an oligo-glycine moiety to facilitate radiolabeling by reducing steric hindrance, (2) an Arg-Asp pair with opposite charges to increase hydrophilicity, and (3) an Asn to serve as a hydrophilic spacer.

In the present study, a hydrophilic linker of GGGRDN was conjugated to the GPC3-targeted TP to form a new PET probe (Al[^{18}F]F-GP2633). The binding assay showed that the addition of the linker slightly enhances the GPC3 binding affinity. The retention time on analytical HPLC and octanol/water partition coefficient confirmed that Al[^{18}F]F-GP2633 is more hydrophilic than Al[^{18}F]F-GP2076, a PET probe without the hydrophilic linker. In addition, Al[^{18}F]F-GP2633 showed excellent specificity of GPC3 binding at cellular level, and good stability *in vitro* and *in vivo*. As compared to Al[^{18}F]F-GP2076, Al[^{18}F]F-GP2633 significantly reduce hepatobiliary excretion and achieve a higher T/L ratio for PET imaging

at all measured time points (30, 60, and 120 min) (Figs. 4 and 5). In addition, slightly increased uptake of Al[^{18}F]F-GP2633 in GPC3-positive HepG2 tumors was also observed as compared to Al[^{18}F]F-GP2076 (Fig. 5). As expected, Al[^{18}F]F-GP2633 showed minimal uptake in GPC3-negative McA-RH7777 tumors. The immunohistochemistry analyses confirmed the GPC3 expression levels in HepG2 and McA-RH7777 tumors, which are consistent with the results form PET imaging. For the radiosynthesis of Al[^{18}F]F-GP2633, a single-step method was achieved by using the Al[^{18}F]F chelation approach. The purification of Al[^{18}F]F-GP2633 without HPLC further simplifies the radiosynthesis procedure. The results demonstrated that the radiosynthesis of Al[^{18}F]F-GP2633 was simple, fast, and efficient with good specific activity of final product.

Overall, our study demonstrated that Al[^{18}F]F-GP2633 is a GPC3-specific probe with favorable PK for PET imaging in HCC. Convenient preparation, excellent GPC3 specificity in HCC, and promising excretion profile of Al[^{18}F]F-GP2633 warrant further translational studies.

Conclusion

New F-18-labeled GPC3-targeted peptides have been successfully developed for PET imaging of GPC3 expression in HCC-bearing mice. The PET probe (Al[^{18}F]F-GP2633) with a hydrophilic linker exhibited better binding affinity to GPC3, enhanced HepG2 tumor uptake, and improved T/L contrast, as compared to the probe (Al[^{18}F]F-GP2076) without the hydrophilic linker. The preclinical data in this study demonstrated that Al[^{18}F]F-GP2633 is a promising PET probe for future clinical translation. PET imaging with a GPC3-specific probe would allow clinicians to early detect GPC3-targeted HCC as well as accurately assess tumor response to GPC3-targeted therapy.

Supplementary Material

Refer to Web version on PubMed Central for supplementary material.

Acknowledgements.

The authors thank Penghui Sun and Meng Wang for their helpful technical assistance.

Funding information. This work was supported by the USC Research Center for Liver Diseases Pilot Funding (NIH Grant No. P30 DK048522), the National Natural Science Foundation of China (81371591 and 81873905), and the Natural Science Foundation of Guangdong Province (2014A030313311).

References

1. Bray F, Ferlay J, Soerjomataram I, Siegel RL, Torre LA, Jemal A (2018) Global cancer statistics 2018: GLOBOCAN estimates of incidence and mortality worldwide for 36 cancers in 185 countries. CA Cancer J Clin 68:394–424 [PubMed: 30207593]
2. Llovet JM, Zucman-Rossi J, Pikarsky E, Sangro B, Schwartz M, Sherman M, Gores G (2016) Hepatocellular carcinoma. Nat Rev Dis Primers 2:16018 [PubMed: 27158749]
3. Siegel RL, Miller KD, Jemal A (2018) Cancer statistics, 2018. CA Cancer J Clin 68:7–30 [PubMed: 29313949]
4. McGlynn KA, Petrick JL, London WT (2015) Global epidemiology of hepatocellular carcinoma: an emphasis on demographic and regional variability. Clin Liver Dis 19:223–238 [PubMed: 25921660]

5. Golabi P, Fazel S, Otgonsuren M, Sayiner M, Locklear CT, Younossi ZM (2017) Mortality assessment of patients with hepatocellular carcinoma according to underlying disease and treatment modalities. Medicine 96:e5904 [PubMed: 28248853]
6. Waghray A, Murali AR, Menon KN (2015) Hepatocellular carcinoma: from diagnosis to treatment. World J Hepatol 7:1020–1029 [PubMed: 26052391]
7. Wagner HN Jr, Conti PS (1991) Advances in medical imaging for cancer diagnosis and treatment. Cancer 67:1121–1128 [PubMed: 1991270]
8. Dulku G, Dhillon R, Goodwin M, Cheng W, Kontorinis N, Mendelson R (2017) The role of imaging in the surveillance and diagnosis of hepatocellular cancer. J Med Imaging Radiat Oncol 61:171–179 [PubMed: 27981791]
9. Yang K, Zhang XM, Yang L, Xu H, Peng J (2016) Advanced imaging techniques in the therapeutic response of transarterial chemoembolization for hepatocellular carcinoma. World J Gastroenterol 22:4835–4847 [PubMed: 27239110]
10. Kornberg A, Schernhammer M, Friess H (2017) ^{18}F-FDG-PET for assessing biological viability and prognosis in liver transplant patients with hepatocellular carcinoma. J Clinic Transl Hepatol 5:224–234
11. Capurro MI, Shi W, Sandal S, Filmus J (2005) Processing by convertases is not required for glypican-3-induced stimulation of hepatocellular carcinoma growth. J Biol Chem 280:41201–41206 [PubMed: 16227623]
12. Filmus J, Capurro M, Rast J (2008) Glypicans. Genome Biol 9:224 [PubMed: 18505598]
13. Capurro M, Wanless IR, Sherman M, Deboer G, Shi W, Miyoshi E, Filmus J (2003) Glypican-3: a novel serum and histochemical marker for hepatocellular carcinoma. Gastroenterology 125:89–97 [PubMed: 12851874]
14. Nakatsura T, Yoshitake Y, Senju S, Monji M, Komori H, Motomura Y, Hosaka S, Beppu T, Ishiko T, Kamohara H, Ashihara H, Katagiri T, Furukawa Y, Fujiyama S, Ogawa M, Nakamura Y, Nishimura Y (2003) Glypican-3, overexpressed specifically in human hepatocellular carcinoma, is a novel tumor marker. Biochem Biophys Res Commun 306:16–25 [PubMed: 12788060]
15. Qi XH, Wu D, Cui HX et al. (2014) Silencing of the glypican-3 gene affects the biological behavior of human hepatocellular carcinoma cells. Mol Med Rep 10:3177–3184 [PubMed: 25270552]
16. Zhou F, Shang W, Yu X, Tian J (2017) Glypican-3: a promising biomarker for hepatocellular carcinoma diagnosis and treatment. Med Res Rev 38:741–767 [PubMed: 28621802]
17. Wu Y, Liu H, Ding H (2016) GPC-3 in hepatocellular carcinoma: current perspectives. J Hepatocell Carcinoma 3:63–67 [PubMed: 27878117]
18. Yang X, Liu H, Sun CK, Natarajan A, Hu X, Wang X, Allegretta M, Guttmann RD, Gambhir SS, Chua MS, Cheng Z, So SK (2014) Imaging of hepatocellular carcinoma patient-derived xenografts using ^{89}Zr-labeled anti-glypican-3 monoclonal antibody. Biomaterials 35:6964–6971 [PubMed: 24836949]
19. Sham JG, Kievit FM, Grierson JR, Miyaoka RS, Yeh MM, Zhang M, Yeung RS, Minoshima S, Park JO (2014) Glypican-3-targeted ^{89}Zr PET imaging of hepatocellular carcinoma. J Nucl Med 55:799–804 [PubMed: 24627434]
20. Sham JG, Kievit FM, Grierson JR, Chiarelli PA, Miyaoka RS, Zhang M, Yeung RS, Minoshima S, Park JO (2014) Glypican-3-targeting F(ab')2 for ^{89}Zr PET of hepatocellular carcinoma. J Nucl Med 55:2032–2037 [PubMed: 25359880]
21. Lee YL, Ahn BC, Lee Y, Lee SW, Cho JY, Lee J (2011) Targeting of hepatocellular carcinoma with glypican-3-targeting peptide ligand. J Pept Sci 17:763–769 [PubMed: 21976137]
22. Chen K, Conti PS (2010) Target-specific delivery of peptide-based probes for PET imaging. Adv Drug Deliv Rev 62:1005–1022 [PubMed: 20851156]
23. Chen K, Chen X (2010) Design and development of molecular imaging probes. Curr Top Med Chem 10:1227–1236 [PubMed: 20388106]
24. Li G, Wang X, Zong S, Wang J, Conti PS, Chen K (2014) MicroPET imaging of CD13 expression using a ^{64}Cu-labeled dimeric NGR peptide based on sarcophagine cage. Mol Pharm 11:3938–3946 [PubMed: 25054774]

25. Chen K, Ma W, Li G, Wang J, Yang W, Yap LP, Hughes LD, Park R, Conti PS (2013) Synthesis and evaluation of ^{64}Cu-labeled monomeric and dimeric NGR peptides for MicroPET imaging of CD13 receptor expression. Mol Pharm 10:417–427 [PubMed: 23190134]
26. Wang Z, Han YJ, Huang S, Wang M, Zhou WL, Li HS, Wang QS, Wu HB (2018) Imaging the expression of glypican-3 in hepatocellular carcinoma by PET. Amino Acids 50:309–320 [PubMed: 29204748]
27. McBride WJ, Sharkey RM, Karacay H et al. (2009) A novel method of ^{18}F radiolabeling for PET. J Nucl Med 50:991–998 [PubMed: 19443594]
28. Chatalic KL, Franssen GM, van Weerden WM et al. (2014) Preclinical comparison of Al^{18}F- and ^{68}Ga-labeled gastrin-releasing peptide receptor antagonists for PET imaging of prostate cancer. J Nucl Med 55:2050–2056 [PubMed: 25413139]
29. Dijkgraaf I, Franssen GM, McBride WJ et al. (2012) PET of tumors expressing gastrin-releasing peptide receptor with an ^{18}F-labeled bombesin analog. J Nucl Med 53:947–952 [PubMed: 22570329]
30. Li ZB, Wu Z, Chen K, Ryu EK, Chen X (2008) ^{18}F-labeled BBN-RGD heterodimer for prostate cancer imaging. J Nucl Med 49:453–461 [PubMed: 18287274]
31. Chen K, Sun X, Niu G, Ma Y, Yap LP, Hui X, Wu K, Fan D, Conti PS, Chen X (2012) Evaluation of ^{64}Cu labeled GX1: a phage display peptide probe for PET imaging of tumor vasculature. Mol Imaging Biol 14:96–105 [PubMed: 21360213]
32. Gao W, Kim H, Feng M, Phung Y, Xavier CP, Rubin JS, Ho M (2014) Inactivation of Wnt signaling by a human antibody that recognizes the heparan sulfate chains of glypican-3 for liver cancer therapy. Hepatology 60:576–587 [PubMed: 24492943]
33. Lee HC, Kim M, Wands JR (2006) Wnt/Frizzled signaling in hepatocellular carcinoma. Front Biosci 11:1901–1915 [PubMed: 16368566]
34. Ma Y, Yang M, Gao H, Niu G, Yan Y, Lang L, Kiesewetter DO, Chen X (2012) Evaluation of fluorine-labeled gastrin-releasing peptide receptor (GRPR) agonists and antagonists by LC/MS. Amino Acids 43:1625–1632 [PubMed: 22354143]
35. Niedermoser S, Chin J, Wangler C, Kostikov A, Bernard-Gauthier V, Vogler N, Soucy JP, McEwan AJ, Schirrmacher R, Wangler B (2015) *In vivo* evaluation of ^{18}F-SiFAlin-modified TATE: a potential challenge for ^{68}Ga-DOTATATE, the clinical gold standard for somatostatin receptor imaging with PET. J Nucl Med 56:1100–1105 [PubMed: 25977461]
36. Hosseinimehr SJ, Tolmachev V, Orlova A (2012) Liver uptake of radiolabeled targeting proteins and peptides: considerations for targeting peptide conjugate design. Drug Discov Today 17:1224–1232 [PubMed: 22781499]
37. Yang M, Gao H, Zhou Y, Ma Y, Quan Q, Lang L, Chen K, Niu G, Yan Y, Chen X (2011) ^{18}F-labeled GRPR agonists and antagonists: a comparative study in prostate cancer imaging. Theranostics 1:220–229 [PubMed: 21544226]

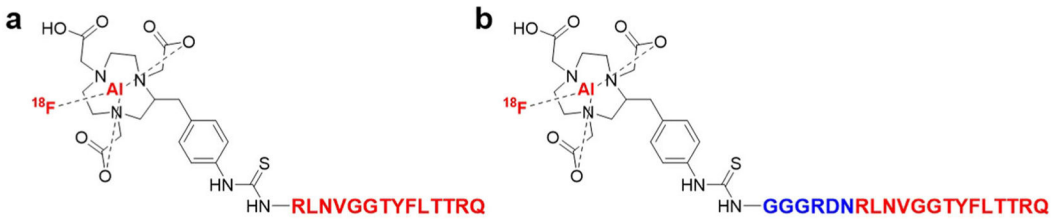

Fig. 1.

Schematic structures of **a** Al[^{18}F]F-GP2076 and **b** Al[^{18}F]F-GP2633.

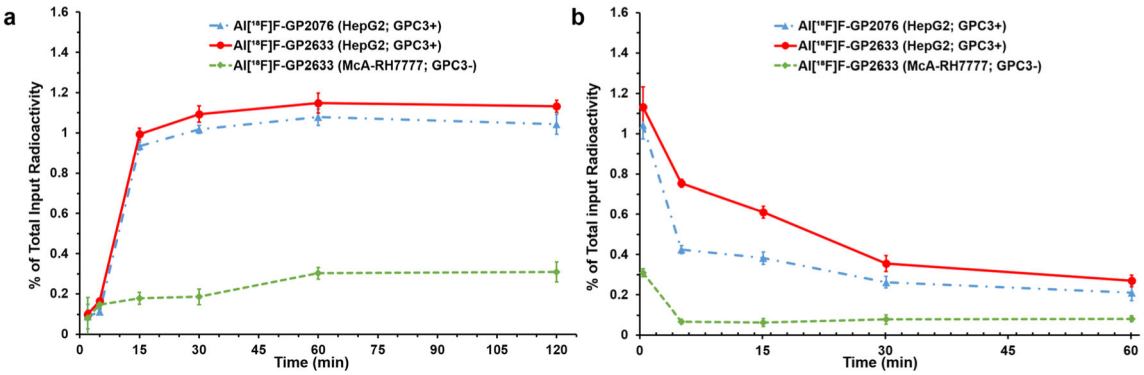

Fig. 2.

Cell uptake and efflux assay. **a** Time-dependent uptake of Al[^{18}F]F-GP2076 (blue line) and Al[^{18}F]F-GP2633 (red line) in GPC3-positive HepG2 cells, and Al[^{18}F]F-GP2633 (green line) in GPC3-negative McA-RH7777 cells (n = 4/group, mean ± SD). **b** Time-dependent efflux of Al[^{18}F]F-GP2076 (blue line) and Al[^{18}F]F-GP2633 (red line) in GPC3-positive HepG2 cells, and Al[^{18}F]F-GP2633 (green line) in GPC3-negative McA-RH7777 cells (n = 4/group, mean ± SD).

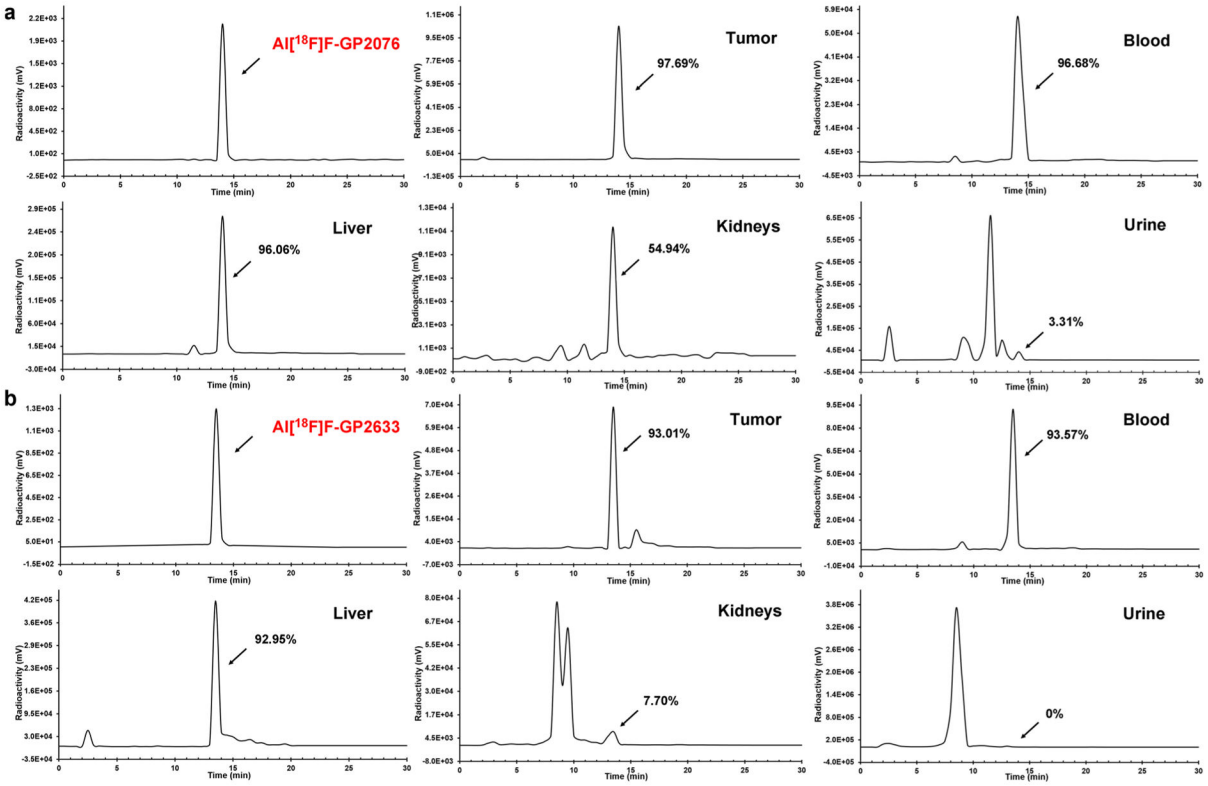

Fig. 3.

Metabolic stability of **a** Al[^{18}F]F-GP2076 or **b** Al[^{18}F]F-GP2633 in HepG2 tumor, blood, liver, kidneys, and urine at 1 h pi. The analytical HPLC profile of Al[^{18}F]F-GP2076 or Al[^{18}F]F-GP2633 is shown as a reference.

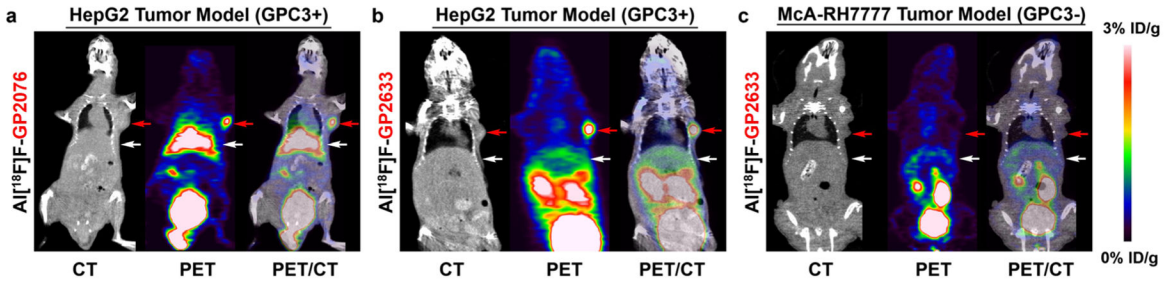

Fig. 4.

MicroPET/CT study of subcutaneous HCC-bearing nude mice after 1 h intravenous (i.v.) injection of Al[^{18}F]F-GP2076 or Al[^{18}F]F-GP2633. Tumors are indicated by red arrows, and livers are indicated by white arrows. Representative decay-corrected whole-body coronal microPET/CT images of nude mice bearing GPC3-positive HepG2 tumor after 1 h i.v. injection of **a** Al[^{18}F]F-GP2076 or **b** Al[^{18}F]F-GP2633. **c** Representative decay-corrected whole-body coronal microPET/CT images of nude mice bearing GPC3-negative McA-RH7777 tumor after 1 h i.v. injection of Al[^{18}F]F-GP2633.

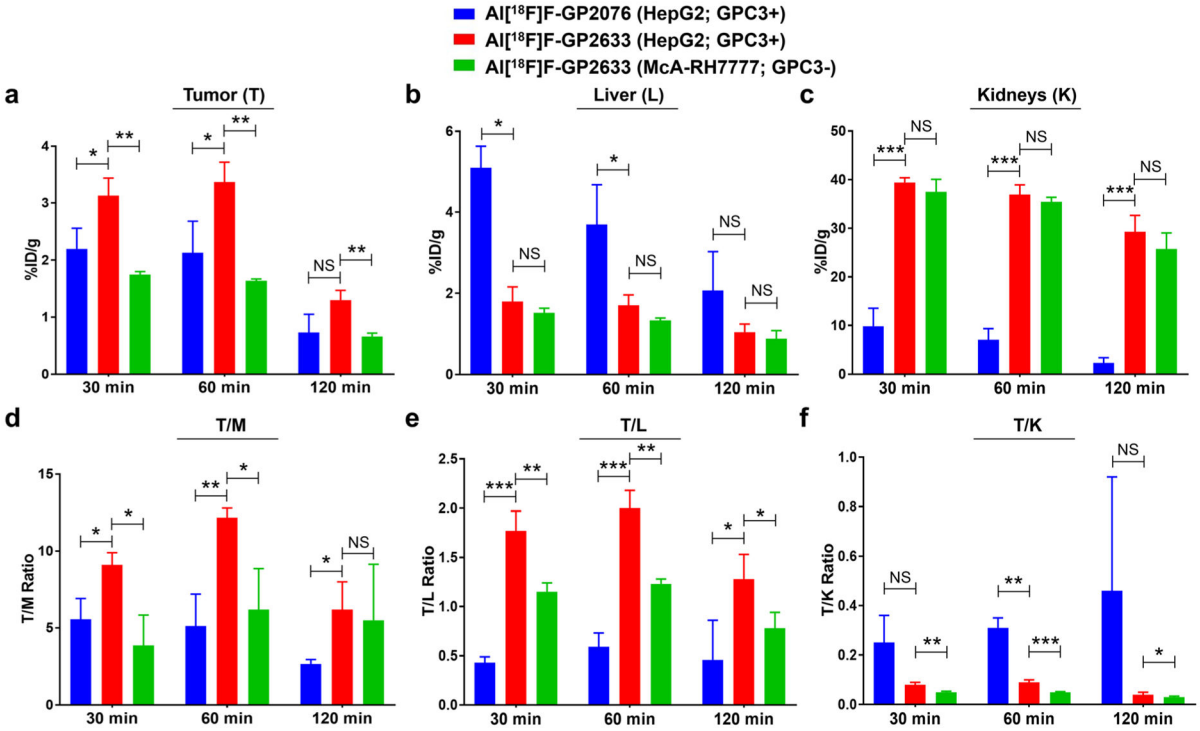

Fig. 5.

Biodistribution of Al[^{18}F]F-GP2076 or Al[^{18}F]F-GP2633 at 30, 60, and 120 min pi in major tissues and organs of subcutaneous HCC-bearing nude mice (n = 3/group; mean ± SD). Blue: Al[^{18}F]F-GP2076 in GPC3-positive HepG2 tumor model; red: Al[^{18}F]F-GP2633 in GPC3-positive HepG2 tumor model; green: Al[^{18}F]F-GP2633 in GPC3-negative McA-RH7777 tumor model. **a** Uptake in tumor (%ID/g). **b** Uptake in liver (%ID/g). **c** Uptake in kidneys (%ID/g). **d** Tumor-to-muscle (T/M) ratio. **e** Tumor-to-liver (T/L) ratio. **f** Tumor-to-kidneys (T/K) ratio. Statistical significance between two groups is shown (*P < 0.05; **P < 0.01; ***P < 0.001; NS, non-significant).

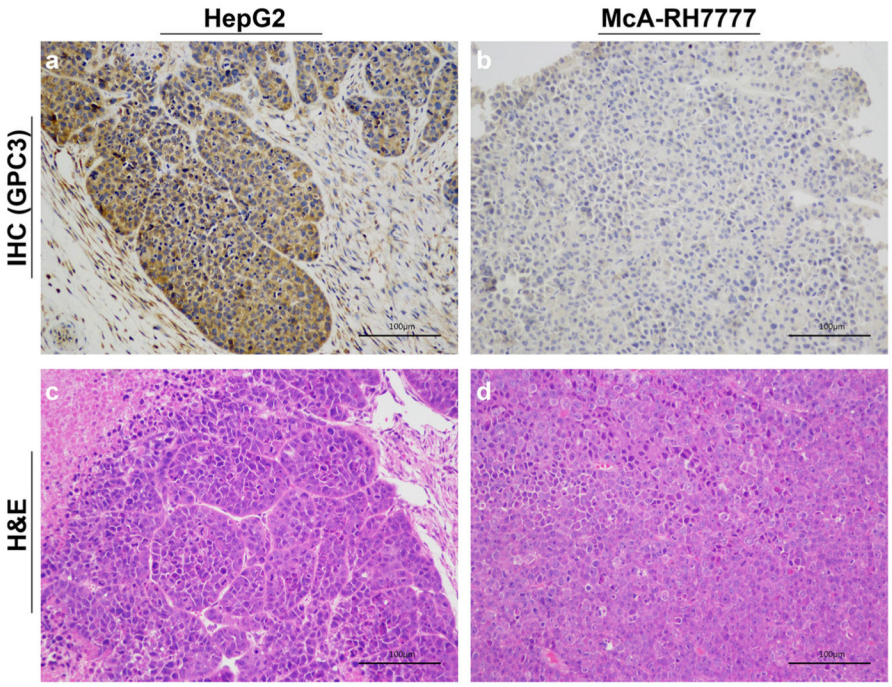

Fig. 6.

Immunohistochemical (IHC) staining of **a** HepG2 tumor and **b** McA-RH7777 tumor for GPC3 and hematoxylin and eosin (H&E) staining of **c** HepG2 tumor and **d** McA-RH7777 tumor (scale bar: 100 μm). The IHC staining confirmed that the HepG2 tumor is GPC3 positive, and the McA-RH7777 tumor is GPC3 negative.